Electronic Supplementary Material (ESI) for Physical Chemistry Chemical Physics.

Supplementary Materials to:

Boson Peak in Silicate Glasses: Insight From Molecular Dynamics

Ahmed El Hamdaoui,[1,*] El Mehdi Ghardi,[2,†] Achraf Atila,[3] Hicham Jabraoui,[4,5] Michael Badawi,[6] Abdellatif Hasnaoui,[7] and Said Ouaskit[1,‡]

[1] *Laboratoire de Physique de la Matière Condensée, Faculté des Sciences Ben M'sik, University Hassan II of Casablanca, B.P 7955, Av Driss El Harti, Sidi Othmane, Casablanca, Maroc*

[2] *Nuclear Futures Institute, Bangor University, Gwynedd, LL57 2DG, United Kingdom*

[3] *Department of Material Science and Engineering, Saarland University, Saarbrücken, 66123, Germany*

[4] *Université Paris-Saclay, NIMBE, CEA, CNRS, F-91191 Gif-sur-Yvette Cedex, France*

[5] *LAAS-CNRS, University of Toulouse, 31077 Toulouse, France*

[6] *Université de Lorraine, F-54000, Nancy, France*

[7] *LS2ME, Faculté Polydisciplinaire Khouribga, Sultan Moulay Slimane University of Beni Mellal, B.P 145, 25000 Khouribga, Morocco*

(Dated: October 24, 2023)

I. COMPUTATIONAL DETAILS

In molecular dynamics simulation, the time evolution of a system of particles is generated by solving the equation of motion and using statistical ensembles. In our simulations, we use different methodologies according to every type of glasses studied in this work.

For the ternary BTS glasses, molecular dynamics simulation was performed on $(BaO)_{0.3}$–$(TiO_2)_X$–$(SiO_2)_{0.7-X}$ glass systems with seven compositions (X = 0, 0.05, 0.10, 0.15, 0.20, 0.25, 0.30) where SiO_2 content was replaced by TiO_2. For each composition, a total number of 4050 atoms were placed randomly in a cubic simulation box ensuring that there is no overlapping between atoms. To model the interatomic interaction in the BTS system, the rigid partial charge ionic model proposed by Pedone et al [1] was used. The atomic compositions, the cubic simulation box cell, and the potential parameters are reported in our earlier work [2].

The CAS simulation was performed on different compositions $(CaO\text{-}SiO_2)_{1-X}$–$(Al_2O_3)_X$ where X is the Al_2O_3 molar fraction (X = 0, 0.05, 0.10, 0.15, 0.20, 0.25, 0.30). To simulate the atomic interaction, we used the Born-Mayer-Huggins (BMH) potential with the parameterization of Bouhadja et al.[3].The glass preparation and the potential parameters used in this work for CAS is described in details in Atila et al. [4].

Concerning modifier oxides, we performed the molecular dynamics simulations on $(M_2O)_x$–$(SiO_2)_{(1-X)}$ with M = Li,K,Na and X is the concentration (X = 0, 0.05, 0.10, 0.15, 0.20, 0.25, 0.30), the simulated systems consist of a number of atoms N=9600 placed in an initial cubic box of size L 50 Å, this size has proven to be sufficient to study this kind of systems while keeping the cost in computation time at a reasonable level. Details on the number of each species relative to the compositions and the final densities of the glasses obtained are described in Tab. II. To describe the interactions of the studied systems, the potential recently developed by Sundararaman et al. [5] (SHIK) was used. This potential describes the short-range interactions under the Buckingham expression taking into account the long-range Coulomb interactions by means of Wolf truncation method [6].To take into account the oxidation state of atoms, partial charges have been assigned to each type of cation (Si, M, with M: [Li, Na, K]) in the system which subsequently allows us to deduce the oxygen

* Corresponding Authors: elhamdaouiahmed96@gmail.com

† m.ghardi@bangor.ac.uk

‡ s.ouaskit@gmail.com

charge as a function of the composition of the glass by the relation:

$$q_O = \frac{(1-X)q_{Si} + (2q_M.X)}{(X-2)} \tag{1}$$

TABLE I: Number of atoms, densities for the different compositions of the studied glasses. The experimental densities were collected from the work of Shawn et al. [7] for LS glasses, of Jabraoui et al.[8] for NS glasses and of Ghardi et al. [9] for KS glasses.

Samples		Composition	Number of atoms			Density	
ID	M_2O	x (%)	O	Si	Li/Na/K	MD (g/cm^3)	Exp (g/cm^3)
SiO_2	—	0	6400	3200	0	2.220	2.203
LS5	Li_2O	5	6240	3040	320	2.230	—
LS10		10	6080	2880	640	2.265	2.246
LS15		15	920	2720	960	2.309	2.269
LS20		20	5760	2560	1280	2.336	2.292
LS25		25	5600	2400	1600	2.366	2.314
NS5	Na_2O	5	6240	3040	320	2.289	2.246
NS10		10	6080	2880	640	2.325	2.293
NS15		15	5920	2720	960	2.374	2.334
NS20		20	5760	2560	1280	2.402	2.370
NS25		25	5600	2400	1600	2.458	2.406
NS30		30	5440	2240	1920	2.513	2.433
KS5	K_2O	5	6240	3040	320	2.312	2.257
KS10		10	6080	2880	640	2.364	2.323
KS15		15	5920	2720	960	2.401	2.354
KS20		20	5760	2560	1280	2.453	2.395
KS25		25	5600	2400	1600	2.467	2.425
KS30		30	5440	2240	1920	2.475	2.437

The cut-off radius for the short-range interactions was chosen to be 8.0 Å. Long-range Coulomb interactions were calculated using the Ewald summation method with a cut-off

radius of 12 Åfor the real part, with a desired relative error for lower forces of 10^{-6}. The simulation was then carried out with periodic boundary conditions and an integration time step of 1 fs. To prepare the glasses, all samples were equilibrated using an NPT ensemble for 1 ns at T = 3500 K, followed by another 100 ps simulation in the NVT ensemble at the same temperature. These steps were necessary to obtain a liquid in which the system had totally lost the memory of its initial state. Then, a rapid cooling (10^{12} K / s) was carried out in the NPT assemble, to obtain the glassy state at room temperature (300 K). Finally, the structures in the glassy state were relaxed for 100 ps in the NVT ensemble to produce a structure for data analysis in room temperature. During this melt-quench-expansion process, the system pressure was kept constant at 0 GPa. The temperature and pressure were controlled using the Nose-Hoover thermostat and barostat [10, 11].The densities of the simulated glasses are slightly higher than the founded experimental data, as reported in Tab. I, by up to 5%, which is within the range of the simulated glasses with other potentials. Additionally, the trend is in good agreement with the experimental data [9, 12–14]. This difference is due to the fact that the simulation technique may not be able to perfectly replicate the conditions under which the experimental glasses were manufactured, such as the cooling rate (1200K/s), which differs greatly between simulation and reality. The Debye equation or Fourier transform of the radial distribution function can be used to get the structural factor. This latter method is often used to compare experiments and simulations directly. The static structural factor is mostly employed in this work to investigate medium range order. The structural factor is expressed by the following equation:

$$S(q) = 1 - \rho \int_0^\infty (g(r) - 1) exp(iqr)\, dr \tag{2}$$

The structure of the produced glasses was evaluated by calculating the structure factors as presented in Fig. 1.as demonstrated in this figure the structure factor of our samples are in good agreement with the experimental data for pure silica, LS and NS, and simulation data available for other studied systems [15–19]. The fractions of the Q_n units for the binary systems are also presented in Fig. 2. Our results are in good agreement with the results reported previously [5, 20]. Concerning the Q_n units fractions in ternary systems BTS and CAS the results are already reported in Ghardi et al. and Atila et al. respectively [2, 4].

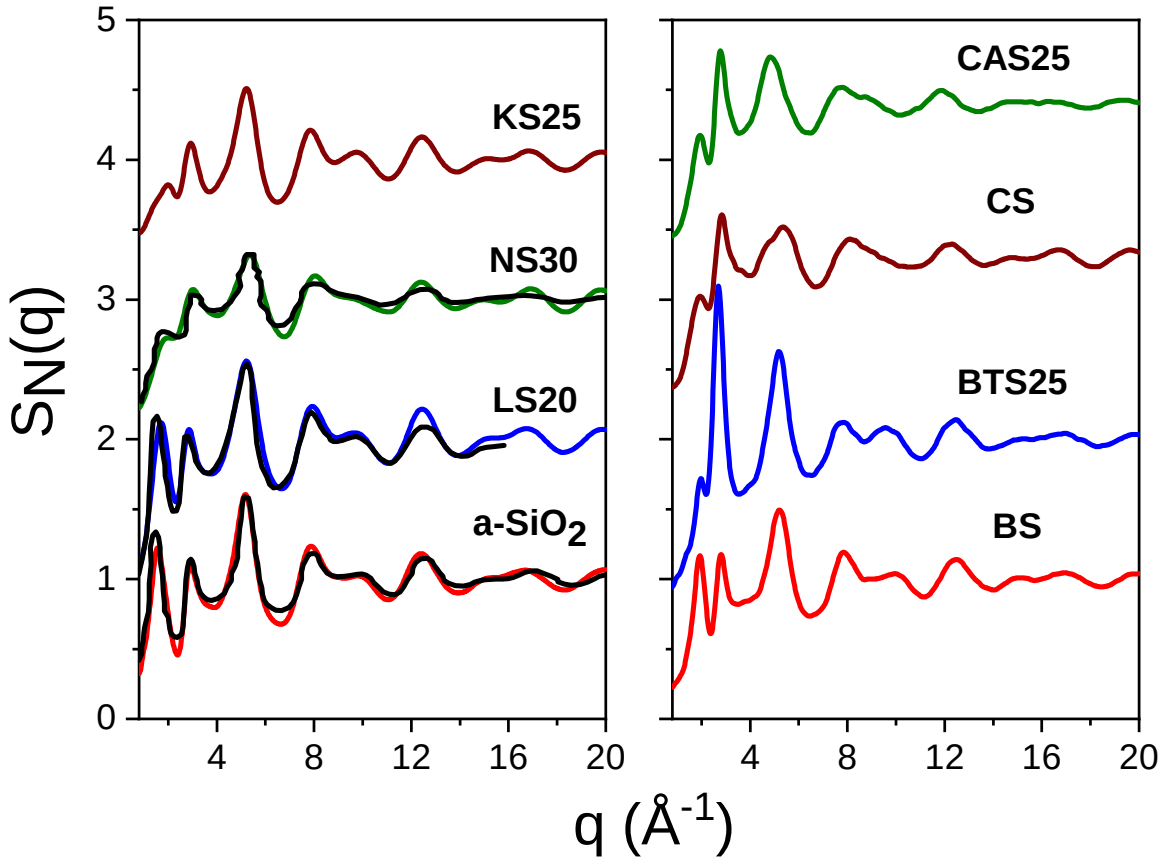

FIG. 1: Structur factors for all studied systems for pure silica and LS20 and NS30 with experimental data (black lines), the experimental data are from Johnson et al [15], LS from Uhlig et al.[16], and NS from Molnar et al. [17]. The compositions are chosen based on the experimental data availability. the 25% composition was chosen for all other systems.

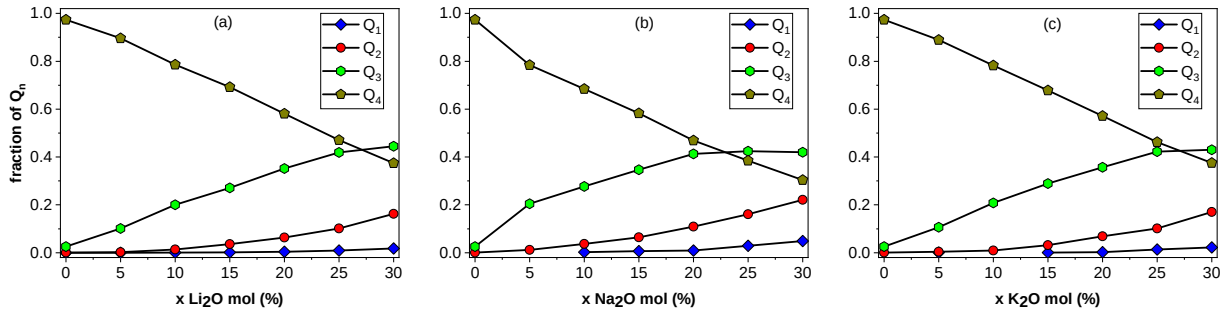

FIG. 2: Q_n units fractions in different compositions for all binary systems: (a) for lithium silicate (LS), (b) for sodium silicate (NS), and (c) for potassium silicate (KS).

II. VDOS AND BP CALCULATION:

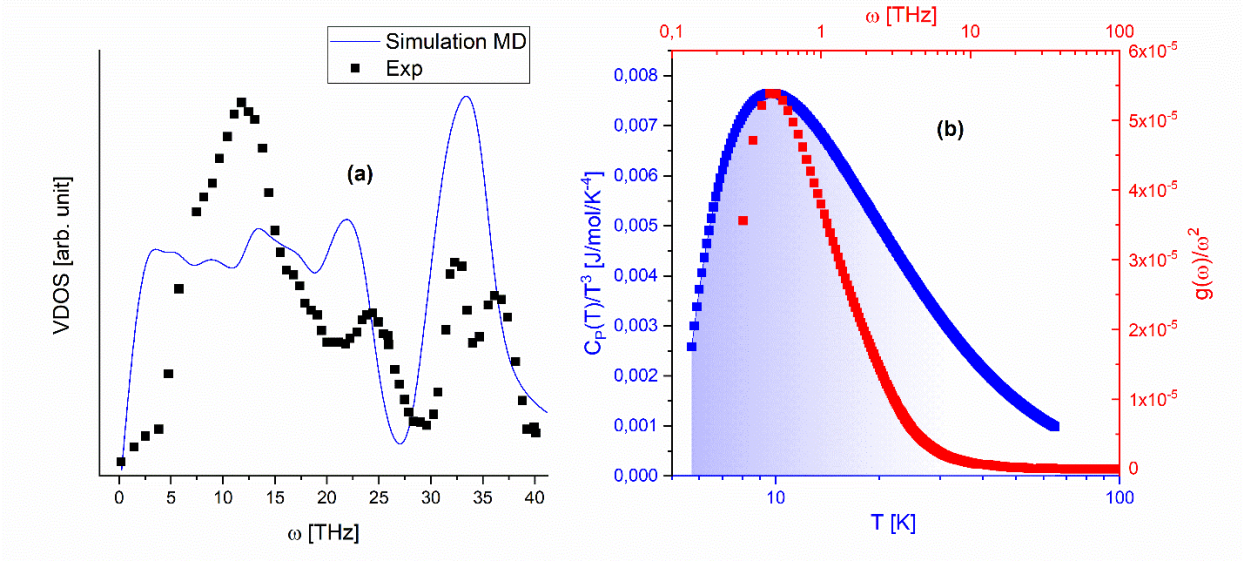

FIG. 3: Vibrational state densities (VDOS) of amorphous silica obtained by simulation (blue line) and inelastic neutron scattering [21] (in black square). (b) The BP observed in heat capacity and VDOS of the simulated silica model.

We computed the vibrational spectrum of pure silica and plotted the simulated result in Fig. 3. from this calculated VDOS the heat capacity using this equation:

$$C_v = 3NK_B \int \frac{\hbar}{2K_BT} \frac{g(\omega)}{sinh^2(\frac{\hbar\omega}{2K_BT})} \tag{3}$$

the BPs were estimated from the normalized VDOS ($g(\omega)/\omega^2$) and heat capacity C_v/T^3 as shown in fig. 3. Regarding this region ($\approx$ 1THz,10K), many interpretations of the nature of the vibrations and their origin have been suggested [22–25]. According to Horbach et al. [26], the strong presence of the BP in amorphous silica is due to the strong coupling of the transverse acoustic excitations and the longitudinal part. The well-known general agreement is that the transverse character is the dominant aspect in the hybridization between the transverse and longitudinal excitations observed in this frequency region [25].

The main characteristics of the vibrational density of state (VDOS) shown in Fig. 3 (wide band at low frequencies between 0 and 25 THz separated by a gap of 1 up to 2 THz from the upper band) are similar to that reproduced by several models of silica, constructed by well-established potentials [5, 12, 27–29] The agreement between the two spectra is sufficiently

TABLE II: Boson Peak frequencies with composition for all studied glasses.

x (%)	LS	NS	KS	BTS	CAS
0	0.44996	0.44996	0.44996	0.98257	1.3683
5	0.34997	0.59994	0.34997	0.95808	1.05785
10	0.34997	0.59994	0.34997	1.10232	1.34451
15	0.44996	0.24998	0.29997	1.1589	1.53351
20	0.39996	0.39996	0.29997	1.16626	1.63617
25	0.44996	0.39996	0.19998	1.18302	1.50802
30	0.59994	0.44996	0.39996	1.21661	1.34501

acceptable to identify the vibrational properties of the simulated glass. An obvious flaw in the calculated VDOS is the presence of irregularities at low frequencies. These irregularities are in some parts artifacts due to the lack of sampling in the reciprocal space.

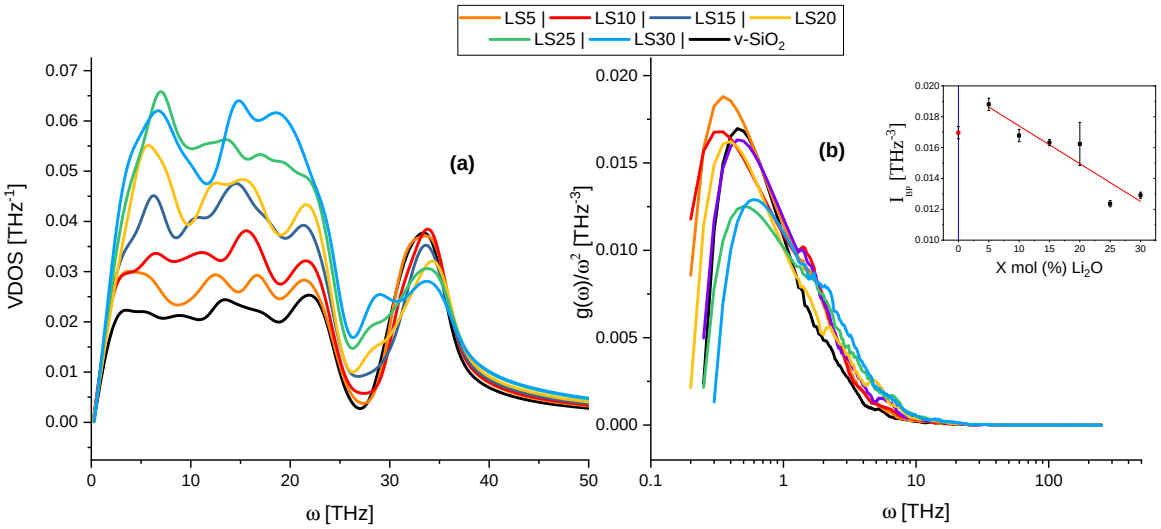

FIG. 4: (a) VDOS of the different compositions of LS glasses. (b) the BP extracted from VDOS. In the inset, the variation of its intensity as a function of the Li_2O content, the point with the vertical line is for pure silica which is used as reference.

On the other hand, Fig. 4b shows the compositional dependence of the BP. A fluctuating behavior according to the composition is observed for this peak. The main observation that can be linked to the effect of Li_2O is the decrease in the intensity of this peak and its shift

to higher frequencies. The decrease in BP is generally related to the decrease in instabilities caused by the disordered nature of the structure [30]. Given the strong ionic character of the Li–O bond, LS glasses become more and more rigid depending on the composition, and this, therefore, constrains the silicate regions of the network to be more stable.

For the sodium silicate, the BP is shown in Fig. 5b. In contrast to LS glasses, the BP increases in intensity with the content of the modifier, leading to the appearance of vibration modes in the low-frequency region. One possible explanation for this observation may be related to the low stiffness of the Na–O bond.

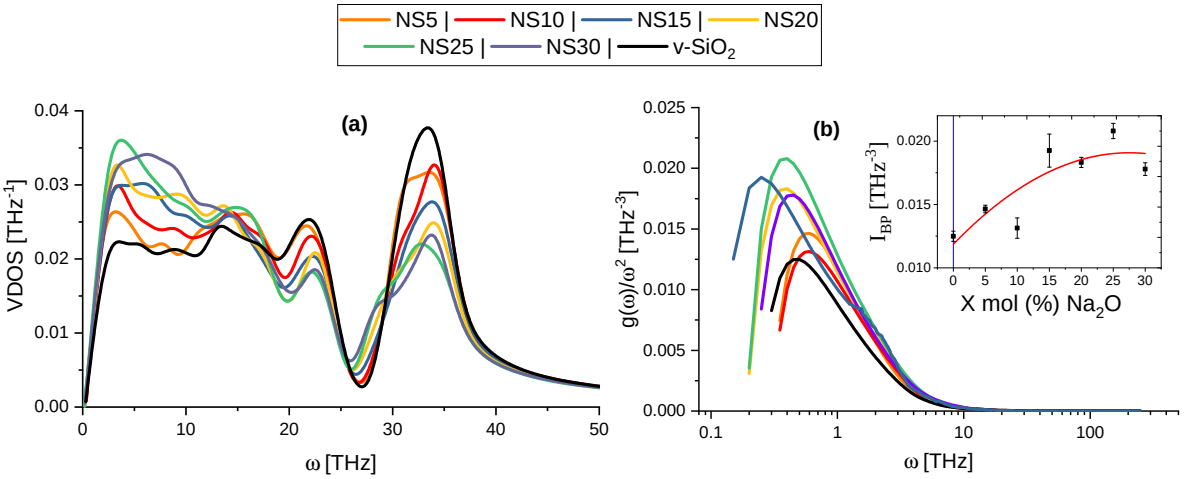

FIG. 5: (a) VDOS of the different compositions of NS glasses. (b) the BP derived from VDOS. In the inset the variation of its intensity as a function of the Na_2O content, the point with the vertical line is for pure silica which is used as reference.

The effect of K_2O content on VDOS and the BP of KS glasses is demonstrated in Fig. 6. Similarly to those NS glasses, the effect of K_2O on the lower and upper bands is described by a decrease in vibrational modes in both bands up to the low-frequency region between 1 and 10THz, where potassium adds more new modes Fig. 6a. The BP in Fig. 6b also demonstrates a similar behavior to that of NS glasses with a general tendency to intensify. The results and the general trend of the effect of the composition are in agreement with available data [31].

The general description of the BP behavior as a function of the alkali content in the silica network limits the comparison between different modifiers to the degree of polymerization. Indeed, the latter is exceeded by the strongest influence exerted by the size of the alkali

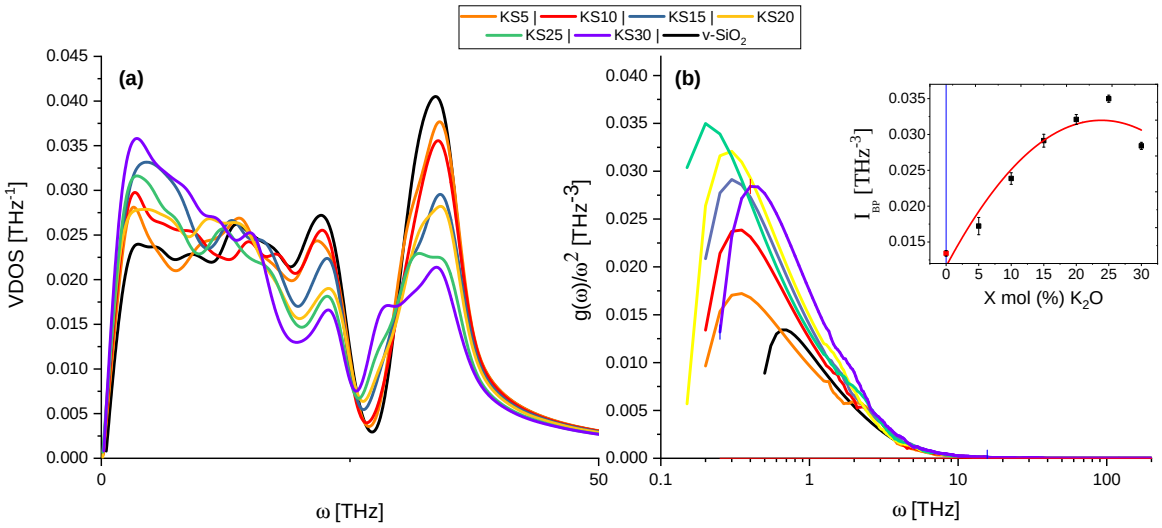

FIG. 6: (a) VDOS of the different compositions of KS glasses. (b) the BP derived from VDOS. In the inset the variation of its intensity as a function of the K_2O content, the point with the vertical line is for pure silica which is used as reference.

cations, which shows that these elements actively participate in the localized vibrations associated with the BP. Consequently, the SiO_4 tetrahedra involved in the *Floppy* modes include non-bridging and bridging oxygen. This was demonstrated by a Raman spectroscopic study of di- and tri-silicates of Li, Na, Rb, and Cs [32] where the frequency of this peak was found to scale approximately as the square root of the alkali cation mass.

A more complete picture is provided by the calorimetric data of Richet [33], thanks to which quantitative comparisons are made for a wider composition range. The Li cations are more strongly bound to oxygen, tighten the network and cause a decrease in the intensity of the BP, which is higher for more depolymerized structures. In contrast, Na and K cations are weakly bound to the glass-forming regions causing the opposite effect. These trends are observed by the inelastic neutron scattering study by Harris et al. [34] according to which the substitution of K^+ for Li^+ results in an improvement in the floppy modes caused by a less well-defined environment of the alkaline cation when the size of their sites are increasing. But the absence of difference between $LiKSi_2O_5$ and $K_2Si_2O_5$ reported in this neutron study still needs to be confirmed as it is hardly compatible with the large differences shown by the LS, NS, and KS glasses.

In Fig. 7b, the effect of alumina on the intensity of the BP is shown for the different compositions of CAS glasses. As in the case of LS glasses, adding Al_2O_3 tends to decrease

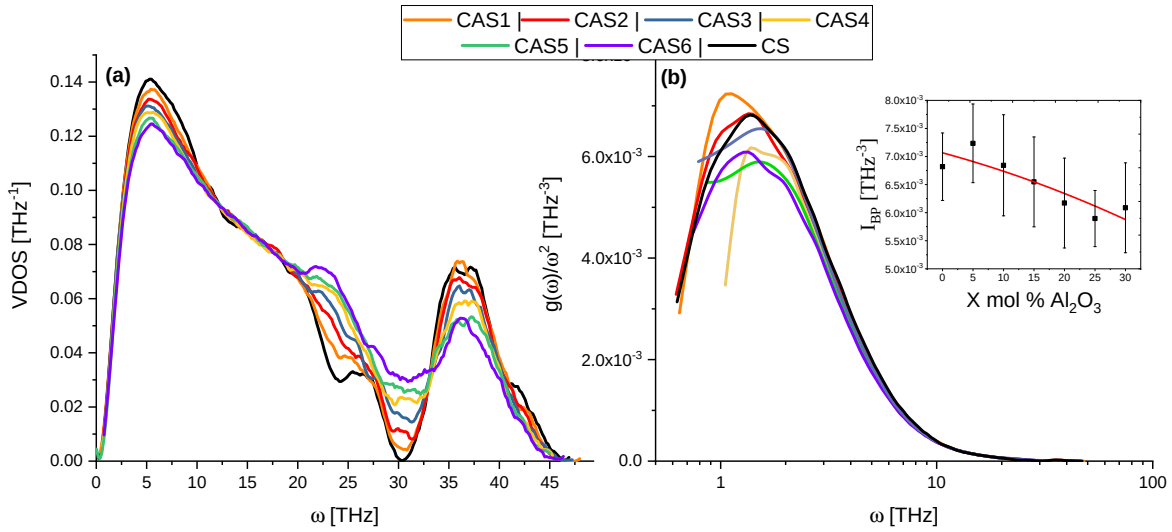

FIG. 7: (a) VDOS of the different compositions of CAS glasses. (b) the BP derived from VDOS. In the inset the variation of its intensity as a function of the Al_2O_3 content.

and shift the peak towards higher frequencies.

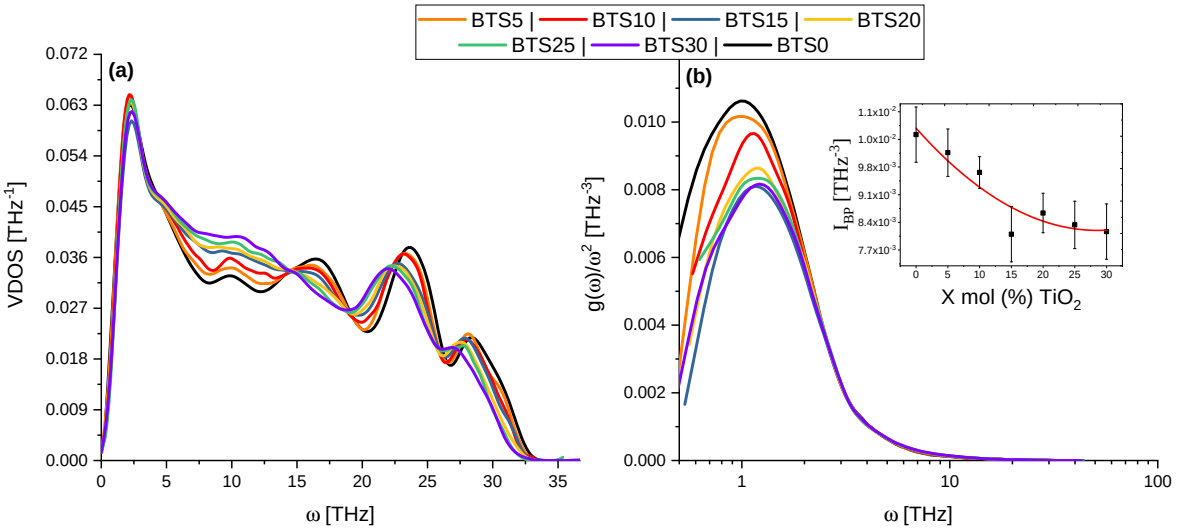

FIG. 8: VDOS and BP for the BTS. (a) VDOS of the different compositions of BTS glasses. (b) BP derived from VDOS. In the inset the variation of its intensity as a function of the TiO_2 content.

The effect of adding TiO_2 on the BP in BTS glasses is shown in Fig. 10b. The peak intensity tends to decrease with the TiO_2 content, as observed for CAS glasses. The more complex role of Ti^{4+} compared to Al^{4+} cations in forming the glass network with silica does

not affect the general tendency of the BP intensity to decrease. Indeed, as found in our earlier work [2], the increase in the TiO_2 content tends to create more order in the glass and therefore leads to a decrease in the effect of disorder in the creation of the vibrational modes of the BP.

III. VIBRATIONAL MSD CALCULATION:

A very useful approach for studying the dynamics of the system is the MSD of particles in time. this parameter can be defined as the distance traveled by specified particle (atom) or a number of particles (molecule) in a given time. the MSD is given by the equation:

$$MSD(t) = \left\langle |r(t) - r(0)|^2 \right\rangle \tag{4}$$

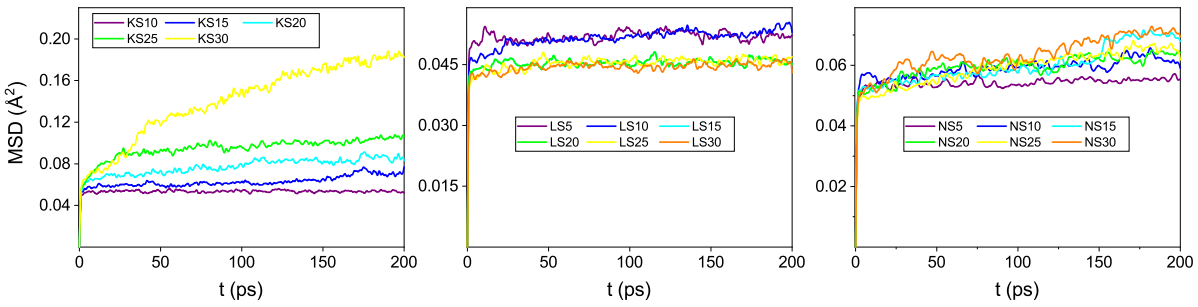

FIG. 9: mean square displacement of Q_4 units in LS, KS, and NS glasses as a function of time.

The MSD was calculated by calculating the trajectories of particles for 200 ps in the NVE ensemble, the trajectories are collected for all atoms and Q_n units in all studied systems every 2 ps. By using this trajectories in the Eq.(3) the MSD and vibrational MSD was calculated.

[1] A. Pedone, G. Malavasi, M. C. Menziani, A. N. Cormack, and U. Segre, A new self-consistent empirical interatomic potential model for oxides, silicates, and silica-based glasses, The Journal of Physical Chemistry B **110**, 11780 (2006).

[2] E. M. Ghardi, A. Atila, M. Badawi, A. Hasnaoui, and S. Ouaskit, Computational insights into

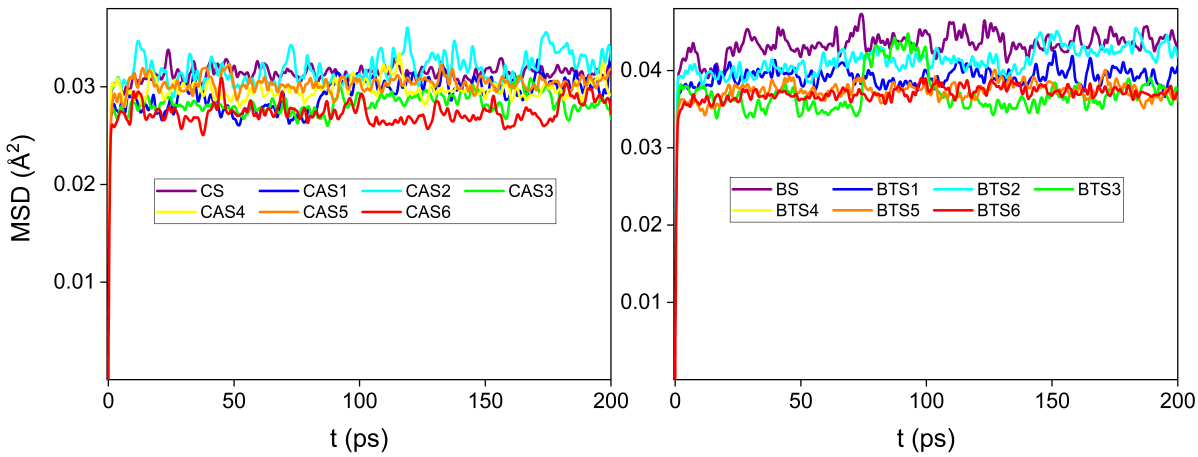

FIG. 10: mean square displacement of Q_4 units in CAS BTS glasses as a function of time.

the structure of barium titanosilicate glasses, Journal of the American Ceramic Society **102**, 6626 (2019).

[3] M. Bouhadja, N. Jakse, and A. Pasturel, Striking role of non-bridging oxygen on glass transition temperature of calcium aluminosilicate glass-formers, The Journal of Chemical Physics **140**, 234507 (2014).

[4] A. Atila, E. M. Ghardi, A. Hasnaoui, and S. Ouaskit, Alumina effect on the structure and properties of calcium aluminosilicate in the percalcic region: A molecular dynamics investigation, Journal of Non-Crystalline Solids **525**, 119470 (2019).

[5] S. Sundararaman, L. Huang, S. Ispas, and W. Kob, New interaction potentials for alkali and alkaline-earth aluminosilicate glasses, The Journal of chemical physics **150**, 154505 (2019).

[6] D. Wolf, P. Keblinski, S. Phillpot, and J. Eggebrecht, Exact method for the simulation of coulombic systems by spherically truncated, pairwise r- 1 summation, The Journal of chemical physics **110**, 8254 (1999).

[7] R. Shaw and D. Uhlmann, Effect of phase separation on the properties of simple glasses ii. elastic properties, Journal of Non-Crystalline Solids **5**, 237 (1971).

[8] H. Jabraoui, Y. Vaills, A. Hasnaoui, M. Badawi, and S. Ouaskit, Effect of sodium oxide modifier on structural and elastic properties of silicate glass, The Journal of Physical Chemistry B **120**, 13193 (2016).

[9] E. M. Ghardi, H. Jabraoui, M. Badawi, A. Hasnaoui, S. Ouaskit, and Y. Vaills, Structure–elasticity relationship of potassium silicate glasses from brillouin light scattering spectroscopy

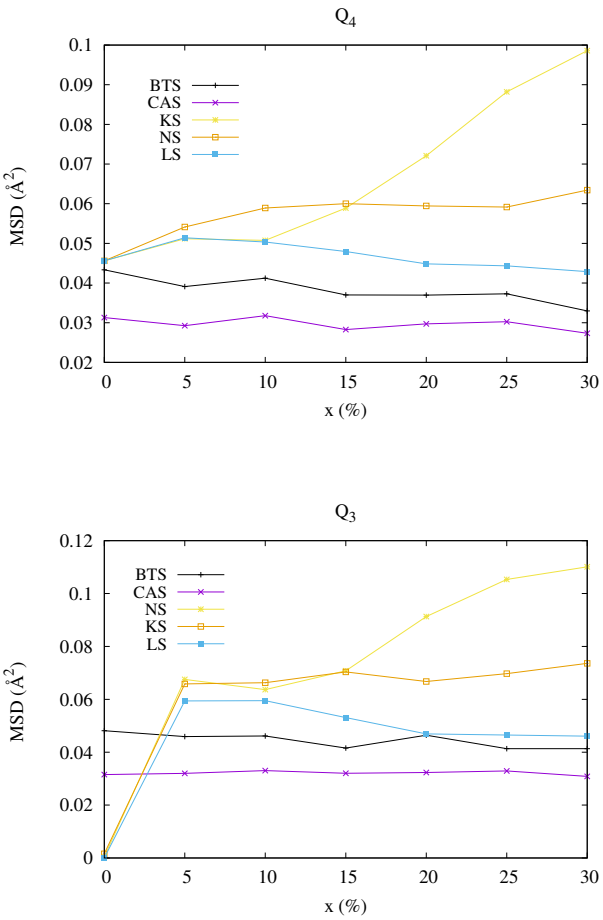

FIG. 11: vibrational mean square displacement of Q_4 units in all studied glasses. the lines are drawn for the guide of the eyes.

and molecular dynamics simulations, The Journal of Physical Chemistry B **124**, 9216 (2020).

[10] S. Nosé, A unified formulation of the constant temperature molecular dynamics methods, The Journal of chemical physics **81**, 511 (1984).

[11] W. G. Hoover, Canonical dynamics: Equilibrium phase-space distributions, Physical review A **31**, 1695 (1985).

[12] A. Pedone, G. Malavasi, A. N. Cormack, U. Segre, and M. C. Menziani, Insight into elastic properties of binary alkali silicate glasses; prediction and interpretation through atomistic simulation techniques, Chemistry of Materials **19**, 3144 (2007).

[13] Y. Yu, B. Wang, M. Wang, G. Sant, and M. Bauchy, Reactive molecular dynamics simulations of sodium silicate glasses—toward an improved understanding of the structure, International

Journal of Applied Glass Science **8**, 276 (2017).

[14] T. S. Mahadevan, W. Sun, and J. Du, Development of water reactive potentials for sodium silicate glasses, The Journal of Physical Chemistry B **123**, 4452 (2019).

[15] P. A. Johnson, A. C. Wright, and R. N. Sinclair, Neutron scattering from vitreous silica ii. twin-axis diffraction experiments, Journal of non-crystalline solids **58**, 109 (1983).

[16] H. Uhlig, M. J. Hoffmann, H.-P. Lamparter, F. Aldinger, R. Bellissent, and S. Steeb, Short-range and medium-range order in lithium silicate glasses, part i: diffraction experiments and results, Journal of the American Ceramic Society **79**, 2833 (1996).

[17] G. Molnár, P. Ganster, J. Török, and A. Tanguy, Sodium effect on static mechanical behavior of md-modeled sodium silicate glasses, Journal of Non-Crystalline Solids **440**, 12 (2016).

[18] J. Du and L. R. Corrales, First sharp diffraction peak in silicate glasses: Structure and scattering length dependence, Physical Review B **72**, 092201 (2005).

[19] J. Du and L. R. Corrales, Compositional dependence of the first sharp diffraction peaks in alkali silicate glasses: A molecular dynamics study, Journal of non-crystalline solids **352**, 3255 (2006).

[20] R. P. Rao, T. Tho, and S. Adams, Ion transport pathways in molecular dynamics simulated lithium silicate glasses, Solid State Ionics **181**, 1 (2010).

[21] M. F. Ando, O. Benzine, Z. Pan, J.-L. Garden, K. Wondraczek, S. Grimm, K. Schuster, and L. Wondraczek, Boson peak, heterogeneity and intermediate-range order in binary sio2-al2o3 glasses, Scientific Reports **8**, 1 (2018).

[22] V. Gurevich, D. Parshin, and H. Schober, Anharmonicity, vibrational instability, and the boson peak in glasses, Physical Review B **67**, 094203 (2003).

[23] M. Klinger and L. Vatova, Origin of boson peak in glasses: Role of atomic soft-mode excitations, Physical Review B **72**, 134206 (2005).

[24] M. Wyart, Scaling of phononic transport with connectivity in amorphous solids, EPL (Europhysics Letters) **89**, 64001 (2010).

[25] A. Chumakov, G. Monaco, A. Monaco, W. Crichton, A. Bosak, R. Rüffer, A. Meyer, F. Kargl, L. Comez, D. Fioretto, *et al.*, Equivalence of the boson peak in glasses to the transverse acoustic van hove singularity in crystals, Physical review letters **106**, 225501 (2011).

[26] J. Horbach, W. Kob, and K. Binder, High frequency sound and the boson peak in amorphous silica, The European Physical Journal B-Condensed Matter and Complex Systems **19**, 531

(2001).

[27] M. Bauchy, Structural, vibrational, and elastic properties of a calcium aluminosilicate glass from molecular dynamics simulations: The role of the potential, The Journal of Chemical Physics **141**, 024507 (2014).

[28] P. Tangney and S. Scandolo, An ab initio parametrized interatomic force field for silica, The Journal of chemical physics **117**, 8898 (2002).

[29] B. J. Cowen and M. S. El-Genk, On force fields for molecular dynamics simulations of crystalline silica, Computational Materials Science **107**, 88 (2015).

[30] A. Hassan, L. Börjesson, and L. Torell, The boson peak in glass formers of increasing fragility, Journal of non-crystalline solids **172**, 154 (1994).

[31] N. F. Richet, Heat capacity and low-frequency vibrational density of states. inferences for the boson peak of silica and alkali silicate glasses, Physica B: Condensed Matter **404**, 3799 (2009).

[32] C. McIntosh, J. Toulouse, and P. Tick, The boson peak in alkali silicate glasses, Journal of Non-Crystalline Solids **222**, 335 (1997).

[33] N. F. Richet, Boson peak of alkali and alkaline earth silicate glasses: Influence of the nature and size of the network-modifying cation, The Journal of Chemical Physics **136**, 034703 (2012).

[34] M. Harris, M. Dove, and J. Parker, Floppy modes and the boson peak in crystalline and amorphous silicates: an inelastic neutron scattering study, Mineralogical Magazine **64**, 435 (2000).